Journal of Catalysis 266 (2009) 236–249

Contents lists available at ScienceDirect

Journal of Catalysis

journal homepage: www.elsevier.com/locate/jcat

Vapour-phase C–C coupling reactions of biomass-derived oxygenates over Pd/$CeZrO_x$ catalysts

Edward L. Kunkes, Elif I. Gürbüz, James A. Dumesic *

Department of Chemical and Biological Engineering, University of Wisconsin, Madison, WI 53706, USA

ARTICLE INFO

Article history:
Received 20 April 2009
Revised 20 May 2009
Accepted 14 June 2009
Available online 17 July 2009

Keywords:
Aldol-condensation
Hydrogenation
Ceria
Zirconia
2-Hexanone
Biofuels

ABSTRACT

Studies of aldol condensation/hydrogenation reactions of 2-hexanone were carried out over Pd/$CeZrO_x$ and $CeZrO_x$ catalysts at temperatures between 573 and 673 K, and pressures of 5–26 bar. These studies were formulated to address the catalytic upgrading to transportation fuels of the mono-functional oxygenated compounds (consisting primarily of C_4–C_6 ketones, alcohols, carboxylic acids and heterocyclics) formed by the catalytic conversion of polyols over a Pt–Re/C catalyst. Characterization by XRD, TPR and NH_3/CO_2–TPD showed that Pd/$CeZrO_x$ catalyst consists of a partially reducible solid solution of cerium and zirconium oxides, and possesses both acidic and basic functionalities. Reaction kinetics studies show that in addition to the expected C_{12} condensation product (7-methyl-5-undecanone), the $CeZrO_x$-based catalysts produce C_{18} and C_9 secondary species, along with light alkanes ($\leqslant C_7$). Low loadings of Pd (e.g., 0.25 wt%) lead to optimal activity and selectivity for the production of C_{12} species. The high apparent activation energy of the formation of C_9 (140 kJ/mol) compared to the formation of C_{12} and C_{18} species (15 and 28 kJ/mol, respectively) indicates that these species may be formed as a result of the decomposition of heavier condensation products. The self-coupling of 2-hexanone was found to be positive order in both 2-hexanone and hydrogen. The addition of primary alcohols and carboxylic acids as well as water and CO_2 to the feed was found to reversibly inhibit the self-coupling activity of 2-hexanone. This inhibition is strongest in the presence of CO_2, and TPSR studies indicate that CO_2 is removed from the surface by conversion to CO in the presence of reduced ceria species.

1. Introduction

Petroleum currently supplies more than 95% of the energy requirements for the US transportation sector [1]. This non-renewable fossil fuel resource is in diminishing supply, and its combustion contributes to the accumulation of CO_2 in the atmosphere, leading to global climate change. However, petroleum-derived fuels possess optimal physical properties with respect to energy density, volatility and hydrophobicity, which allow for efficient storage, distribution and combustion. Biomass-derived fuels have attracted considerable attention as alternatives to petroleum, because they are derived from abundant, renewable resources, and because combustion of these fuels is CO_2 neutral. However, obtaining biomass-derived fuels with the appropriate physical and combustion properties to integrate into the current transportation infrastructure has presented numerous challenges. For example, utilization of the most successful biomass-derived fuel, ethanol, necessitates modifications to the internal combustion engine of the vehicle and the use of bio-diesel requires special precautions in cold climates [2,3].

In our recent work, we have developed a catalytic process that can be tuned to convert biomass-derived carbohydrates to a variety of fuel-grade products, such as light alkenes (C_1–C_4), benzene, substituted aromatics, branched alkenes (C_6–C_{12}) and linear or singly branched alkanes (C_7–C_{12}). This process consists of an initial de-oxygenation step that converts concentrated aqueous solutions of sugars and polyols (40–60%) over a carbon-supported Pt–Re catalyst into hydrophobic mixtures of mono-functional C_4–C_6 alcohols, ketones, carboxylic acids and heterocyclic compounds [4]. The carbon chain length of these monofunctional species is limited to six by the chain length of the parent carbohydrate, i.e., glucose and sorbitol. To produce higher molecular weight species required for gasoline, diesel and jet fuel applications, the mixture of monofunctional species is subsequently subjected to catalytic C–C coupling processes. These coupling processes include (i) ketonization, in which two carboxylic acid molecules react to form a linear ketone, CO_2 and water [5], and (ii) aldol condensation/hydrogenation, in which two ketone or alcohol molecules react to form a heavier branched ketone [6]. The combination of ketonization and aldol condensation/hydrogenation yields C_7–C_{12} linear and branched ketones, which can be converted into fuel-grade alkanes via dehydration/hydrogenation over solid acid supported noble metal catalysts, such as Pt/$NbOPO_4$ [7].

* Corresponding author.
E-mail address: dumesic@engr.wisc.edu (J.A. Dumesic).

0021-9517/$ - see front matter © 2009 Elsevier Inc. All rights reserved.
doi:10.1016/j.jcat.2009.06.014

Ketonization of carboxylic acids has been investigated in the literature using a variety of basic, acidic and amphoteric oxide catalysts, and occurs at temperatures near or higher than 623 K [6,8,9]. We have demonstrated that the carboxylic acids found in the aforementioned carbohydrate-derived mixture of monofunctional species can be ketonized with nearly 100% yield over a $CeZrO_x$ mixed oxide catalyst at temperatures from 623 to 673 K [4]. The combined aldol condensation/hydrogenation of alcohols and ketones has been studied in the literature on metals (Cu and Pd) supported on mixed oxides such as $MgAlO_x$ [5,10] and anion-exchange resins [11] in the temperature range from 423 to 473 K in the presence of hydrogen. This reaction consists of metal-catalyzed dehydrogenation of alcohol groups, followed by base-catalyzed aldol condensation, acid-catalyzed dehydration and subsequent metal-catalyzed hydrogenation of the α–β unsaturated aldol adduct. Hydrogenation of the C=C bond in the dehydrated aldol adduct improves the overall thermodynamics for the process, allowing a greater extent of C–C coupling than aldol condensation/dehydration alone [5,10,12]. Several investigators report that the presence of intermediate strength acidic and basic sites in proximity results in optimal catalytic performance [10,13–15], and the presence of strong acid or basic sites leads to undesirable side reactions that may also lead to coking [16].

Most studies of aldol condensation/hydrogenation have focused on self-condensation of acetone or isopropanol to form MIBK [5,12,17–21], and few reports have been published regarding self-condensation of higher ketones [22] (such as the ones produced from the conversion of carbohydrates on Pt–Re/C). In contrast to acetone, C_{4+} methyl ketones possess a single set of reactive α-hydrogen atoms, resulting in a substantial decline in reactivity when compared to acetone. As a result, higher reaction temperatures are required to achieve appreciable conversion, and appropriate catalysts must be used that are resistant to coking and sintering at these conditions. In this respect, we have reported the self-condensation/hydrogenation of 2-hexanone on a $CuMg_{10}Al_7O_x$ catalyst at 573 K and have shown that even small amounts of carboxylic acids are detrimental to the self-condensation reaction [23]. For this reason, the ketonization reaction provides an efficient means of removing carboxylic acids from the feed prior to aldol condensation/hydrogenation, and we have demonstrated that a catalyst consisting of Pd-supported on $CeZrO_x$ is effective at 623 K for the condensation of ketones present in the ketonized mixture of monofunctional species derived from glucose [4]. The $CeZrO_x$ support was selected because it possesses high lattice oxygen mobility and the ability to interact strongly with supported metals – properties that have been associated with resistance to the formation of carbonaceous species that lead to deactivation [24,25]. Additionally, $CeZrO_x$ contains a combination of acidic and basic functionalities for aldol condensation [26]. Thus, we suggest that ketonization and aldol condensation/hydrogenation can be carried out at comparable operating conditions, and can potentially be integrated into a single reactor system, containing a catalytic bed consisting of $CeZrO_x$ to perform ketonization, followed by a downstream bed of $Pd/CeZrO_x$ to perform aldol condensation/hydrogenation.

In the current work, we explore the possibility of the aforementioned integration between ketonization and aldol condensation/hydrogenation by elucidating the reaction pathways for aldol condensation of a representative ketone (2-hexanone) on Pd/CeZrOx by varying reaction conditions, such as temperature, pressure and space velocity. We show that in addition to the expected C_{12} condensation product (7-methyl-5-undecanone), the catalyst produces C_{18} and C_9 secondary species. We investigate the effect of metal loading and proximity of metal and support on catalytic activity, and we find that low metal loadings lead to optimal activity and selectivity. Additionally, we investigate the effect of other monofunctional oxygenates present in the carbohydrate-derived hydrophobic mixture, such as primary and secondary alcohols, carboxylic acids, heterocyclics and 3-ketones on the self-condensation of 2-hexanone. Furthermore, we study the effects of the ketonization by-products, CO_2 and water, on the downstream condensation reaction, and we probe the interaction of $CeZrO_x$ with CO_2 using temperature-programmed desorption (TPD), temperature-programmed reduction (TPR) and temperature-programmed surface reaction (TPSR) of CO_2. We observe that the addition of oxygenates as well as water and CO_2 all lead to reversible inhibition of the self-condensation activity, and this inhibition is strongest when CO_2 is present in the feed. Through these observations we conclude that it is beneficial to remove water and CO_2 prior to the aldol/condensation hydrogenation step over $Pd/CeZrO_x$.

2. Experimental

2.1. Catalyst preparation

The $CeZrO_x$ support with a 1:1 Ce:Zr molar ratio was prepared via co-precipitation of $Ce(NO_3)_3$ and $ZrO(NO_3)_2$ with NH_4OH (Aldrich) according to Serrano-Ruiz et al. [27]. The $Pd/CeZrO_x$ catalyst was prepared via incipient wetness impregnation of $CeZrO_x$ with an amount of aqueous solution of $Pd(NO_3)_2$ (Aldrich) necessary to obtain nominal metal loadings of 0.05, 0.25 and 1.45 wt%. The catalyst was dried in air at 373 K overnight and calcined in air at 623 K for 2 h. A 0.5 wt% Pd/SiO_2 catalyst was prepared via the same procedure, using a Cab-O-Sil silica gel support.

2.2. Reaction kinetics studies

2-Hexanone, 1-butanol, tetrahydrofuran, heptane, 3-pentanone and butanoic acid were purchased from Sigma–Aldrich and were used without further purification. Hydrogen (99%), helium (99.9%) and 10 mol% CO_2 in helium were purchased from Airgas and used without further purification. The conversions of oxygenated species over $Pd/CeZrO_x$ were carried out at temperatures between 573 and 673 K, pressures of 5–26 bar, and liquid flow rates between 0.02 and 0.08 mL/min. The molar ratio of the gas flow rate to the liquid flow rate was maintained at 5.5, with the exception of reaction order studies. A fixed bed, down-flow reactor consisting of a half-inch stainless steel tube, shown schematically in Fig. 1, was used for all experiments. Quartz wool was used in the lower end of the reactor to keep the catalyst bed in place. The catalyst was mixed with crushed fused quartz granules (Aldrich) in a 2:1 volumetric ratio to maintain bed height. The reactor was heated with an aluminium block that was heated externally by a well-insulated furnace (Applied Test Systems). Type-K thermocouples (Omega) were used to measure the reaction temperature, which was controlled by a PID controller (Love controls) connected to a variable transformer (Tesco). Mass flow controllers (Brooks 5850E) were used to regulate the flow of H_2, He and CO_2 (10 mol% in He) during the experiments. The liquid feed was pumped from a graduated cylinder by an HPLC pump (Lab Alliance series 1) to a needle located at the entrance of the catalyst bed. A back-pressure regulator (GO model BP-60) was used to control the total pressure, which was measured by two gauges at the entrance and the exit of the bed. A gas–liquid separator at room temperature was used to collect the liquid phase for analysis. The catalyst was reduced in situ at 623 K (ramp rate of 0.5 K min^{-1}) for 2 h in flowing H_2 [200 cm^3(STP) min^{-1}]. After the reduction was completed, the temperature and pressure were adjusted and the feed flow was started with flowing H_2 or H_2–He or H_2–CO_2 mixtures. The weight hourly space velocity (WHSV) was calculated for experiments using the mass flow rate of the liquid flow into the

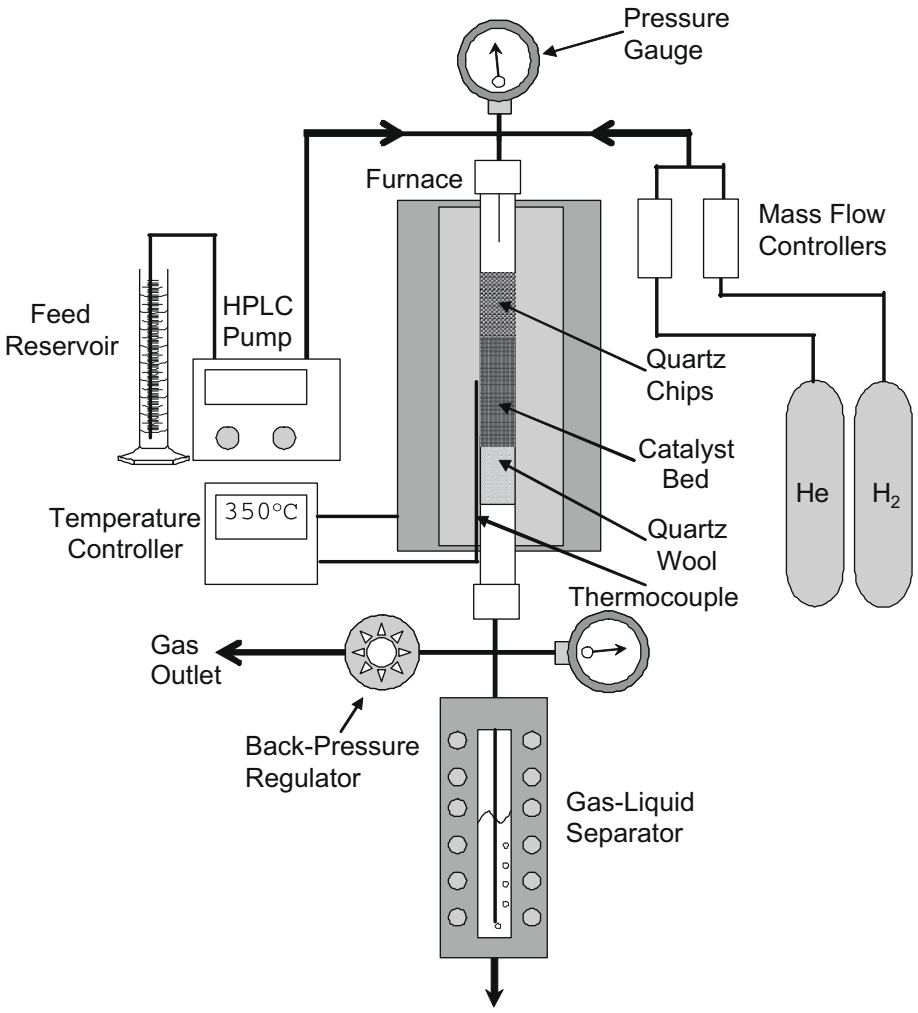

Fig. 1. Reactor system used in reaction kinetics studies.

reactor and the mass of the catalyst used (2 g, except for reaction order studies).

The rate of gas production was measured with a bubble flow meter. An HP GC5890 gas chromatograph, equipped with a Haysep DB 100/120 column (Alltech) and thermal conductivity detector (TCD), was used to quantify CO and CO_2, and an Agilent GC6890, equipped with an Rtx column (Agilent) and a flame ionization detector (FID), was used to quantify gas-phase alkanes. Liquid phase analysis was performed with a Shimadzu GC 2060, equipped with a DB-5 column (Restek) and an FID detector. Unknown species were identified with a Shimadzu 2060 GC/MS with a NIST library of spectra. Some species could not be identified definitively using the library, and their identification was based on the atomic mass of the molecular ion fragment and analogous species reported for acetone condensation. Liquid and gas analysis points were collected every 2–3 h, and steady state was usually achieved after 6 h time-on-stream. At our reaction conditions on Pd-containing catalysts, 2-hexanol was always in equilibrium with 2-hexanone. Therefore, the conversion of 2-hexanone to 2-hexanol was not factored into the total conversion calculation, as given by Eq. 1. The selectivities to reaction products were calculated on a molar carbon basis, as given by Eq. 2. In Eqs. (1) and (2), R represents the molar flow rate, *f* represents reactant conversion, *S* represents the carbon selectivity, and N is the carbon number of a given species. All carbon balances closed to within 10%

$$f_{2\text{-hexanone}} = \left(1 - \frac{R_{2\text{-hexanone\_out}} + R_{2\text{-hexanol\_out}}}{R_{2\text{-hexanone\_in}}}\right) \times 100\% \quad (1)$$

$$S_j = \left(\frac{R_{j\_out} N_j}{\sum_j (R_{j\_out} N_j)}\right) \times 100\%. \quad (2)$$

2.3. Catalyst characterization

2.3.1. CO chemisorption and BET measurements

The adsorption uptakes of carbon monoxide at 300 K were measured on a standard gas adsorption apparatus described elsewhere [28]. The number of surface metal sites was taken to be the irreversible CO uptake. The BET surface area was measured by nitrogen adsorption at liquid nitrogen temperature on the same apparatus.

2.3.2. XRD

X-ray diffraction (XRD) was used to investigate the phase structure of the $Pd/CeZrO_x$ catalyst. A Scintag PAD V X-ray diffractometer with a monochromated CuK_α X-ray tube was used in the diffraction studies. The tube voltage and current were 45 kV and 40 mA, respectively. Diffraction patterns were collected in the 20° to 65° 2θ range, with 0.01° intervals and a dwell time of 2 s.

2.3.3. TPD

Carbon dioxide and ammonia temperature-programmed desorption (TPD) experiments were carried out using an apparatus consisting of a mass flow controller (Teledyne-Hastings) and a tube furnace connected to a variable power-supply and PID temperature controller (Love Controls) with a K-type thermocouple (Omega). The effluent was monitored by a mass spectrometer system consisting of a quadruple residual gas analyzer (Stanford Instruments RGA 200) inside a vacuum chamber. Vacuum was provided by a diffusion pump connected in series to a rotary pump. The effluent was introduced into the vacuum chamber via a constricted quartz capillary, resulting in a pressure of 5×10^{-5} Torr inside the chamber. Dried, unreduced catalyst samples were loaded into a 12.6 mm (0.5 in.) outer diameter, fritted quartz tube reactor. Prior to desorption experiments, 0.3–1 g of catalyst was reduced in flowing hydrogen (100 cm^3(STP) min^{-1}) for 2 h at 623 K. The catalyst was degassed for 1 h in flowing helium (200 cm^3(STP) min^{-1}) at the reduction temperature, and was then cooled to 300 K for CO_2 adsorption and 423 K for NH_3 adsorption, respectively. Carbon dioxide was adsorbed onto the reduced catalysts by exposure to flowing 10 mol% CO_2 in helium (100 cm^3(STP) min^{-1}) for 30 min. Residual CO_2 was removed by purging the catalyst with helium (200 cm^3(STP) min^{-1}) at 300 K for 2 h. Ammonia adsorption was performed in a similar manner as CO_2 adsorption, except that both adsorption and purging steps were performed at 423 K, and a 1 mol% NH_3 in He gas mixture was used. Desorption of CO_2 or NH_3 was performed by heating the catalyst at a rate of 10 K min^{-1} under flowing helium (50 cm^3(STP) min^{-1}) from room temperature to 1073 K for NH_3 or 1123 K for CO_2.

2.3.4. TPR and TPSR measurements

Temperature-programmed surface reaction (TPSR) experiments followed the same procedure as those involving TPD of CO_2, except that the desorption of CO_2 was performed in flowing hydrogen (50 cm^3(STP) min^{-1}). Temperature-programmed reduction (TPR) measurements were performed by heating 0.2–0.3 g of calcined catalyst at 10 K min^{-1} under a 5 mol% H_2 in N_2 mixture (50 cm^3(STP) min^{-1}) to 973 K, and measuring hydrogen consumption with the MS system described above.

3. Results and discussion

3.1. Surface and bulk characterization

The desorption profiles of NH_3 and CO_2 from $CeZrO_x$ and several $Pd/CeZrO_x$ catalysts of various loadings are shown in Fig. 2. These profiles were integrated to obtain the quantities of acidic and basic surface sites, which are reported in Table 1. The values of the irreversible CO uptake and BET areas are also listed out in Table 1. The NH_3 desorption profiles of all catalysts show a single, uniform desorption peak, centered at 570–600 K, suggesting a narrow distribution of acidic sites on the surface. These results are consistent with those obtained by Zhu et al. for NH_3 TPD from $Pt/CeZrO_x$ [29]. The 1.45 wt% Pd catalyst contains nearly 50% more NH_3 adsorption sites than $CeZrO_x$ and the lower loading catalysts. Pokrovski and Bell showed that the presence of a hydrogen-dissociating metal on $CeZrO_x$ causes the reduction of Ce^{4+} into Ce^{3+} via hydrogen spillover, and the presence of Ce^{3+} is shown to increase the acidity of the $CeZrO_x$ surface [30]. In this respect, the 1.45 wt% $Pd/CeZrO_x$ catalyst may contain sufficient concentrations of Ce^{3+} to influence the acidic site properties, as measured by NH_3 TPD.

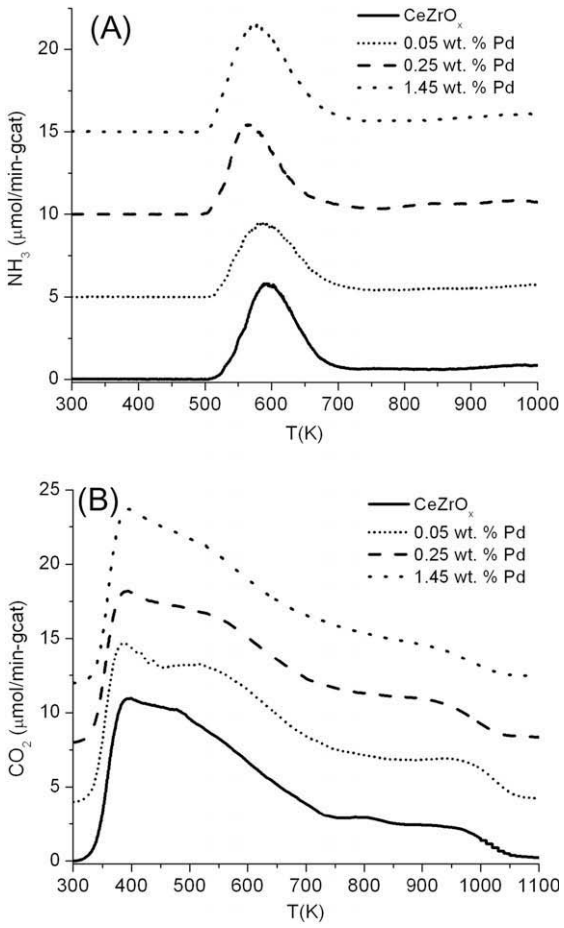

Fig. 2. NH_3 desorption profiles (A) and CO_2 desorption profiles (B) from $CeZrO_x$ and $Pd/CeZrO_x$ catalysts.

The CO_2 desorption profiles show the presence of basic sites of varying CO_2 adsorption strength. These profiles can be divided into three distinct regions representing weak adsorption sites (300–500 K), medium-strength adsorption sites (500–700 K), and strong adsorption sites (700–1000 K). Di Cosimo et al. have correlated TPD and FTIR studies of CO_2 adsorbed on $MgAlO_x$ and have associated the CO_2 desorption temperature with different types of CO_2 binding sites. The weakly binding sites are associated with surface OH groups and the formation of bicarbonate, while the medium-strength sites are associated with M^{x+}–O^{2-} pairs and the formation of bridged and bidentate carbonates. The strongly binding sites are

Table 1
Quantification of metal (CO), basic (CO_2) and acidic sites (NH_3), and BET surface areas of selected catalysts.

Catalyst	CO (irreversible) (μmol/g)	Apparent Pd dispersion (%)[a]	CO_2 (TPD) (μmol/g)	NH_3 (TPD) (μmol/g)	BET area (m^2/g)
$CeZrO_x$	0	–	370	56	130
0.05% $Pd/CeZrO_x$	8	170	390	50	135
0.25% $Pd/CeZrO_x$	18	77	380	54	133
1.45% $Pd/CeZrO_x$	76	57	395	77	139
0.5% Pd/SiO_2	9	20	–	–	–

[a] The Pd dispersion is over-estimated because of CO chemisorption on reduced sites on the support.

associated with low coordination O^{2-} ions and the formation of more strongly bound unidentate carbonates [14]. Several of the aforementioned species have been observed on ZrO_2 [31], and it is probable that the correlation found by Di Cosimo et al. for $MgAlO_x$ may be extended to other oxides such as $CeZrO_x$.

Di Cosimo et al. and Bianchi et al. observed weak CO_2 adsorption sites on CeO_2 and weak- and medium-strength sites on ZrO_2, respectively [21,32]. The presence of stronger CO_2 binding sites on $CeZrO_x$ surface likely results from the surface heterogeneity introduced by substituting Ce ions with Zr^{4+} ions. The addition of Zr to Ce is known to increase the mobility of O^{2-} ions in the lattice [27,33], and is therefore likely to cause higher concentrations of low coordination O^{2-} (associated with surface defects) that strongly bind CO_2. The number and strength of CO_2 binding sites are not influenced significantly by metal loading. This observation is different from that of Nikolopolous et al. who observed that the surface basicity decreases with increasing Pd loading on $MgAlO_x$. Nikolopolous et al. suggest that residual chlorine from the metal precursor ($PdCl_2$) is responsible for this effect [5]. This detrimental effect on basicity was not observed in the present investigation, probably due to the use of a nitrate precursor ($Pd(NO_3)_2$) that decomposed to PdO upon calcination.

The BET surface area is not affected by metal loading in the loading range studied here, suggesting that there is no modification to the pore structure upon metal deposition. The BET surface area (130–140 m^2/g) is consistent with measurements obtained by other investigators on $CeZrO_x$ prepared by the co-precipitation method [27].

Measurements of irreversible CO adsorption show that the CO uptake increases with metal loading. When a reducible oxide support is present (such as CeO_2), reduced sites on the support can contribute to the CO uptake, which normally occurs only on metal sites [34]. This phenomenon is particularly evident in the case of 0.05 wt% $Pd/CeZrO_x$, where the amount of chemisorbed CO appears to exceed the number of Pd atoms in the catalyst. TPR studies in the present work and by others show that hydrogen spillover is responsible for the reduction of surface Ce^{4+} into Ce^{3+}, and this reduction takes place at the interface of the metal and the support [27]. For smaller particles, the ratio of these interfacial sites to metal sites is higher than that for large particles, leading to a greater normalized CO uptake (apparent dispersion). Even though the dispersion measured by CO chemisorption is over-estimated, these results demonstrate that the Pd particle size decreases with lower Pd loadings, since the apparent dispersion increases with decreasing loading, as shown in Table 1. Metal particle sizes were not measured independently, because the objective of the chemisorption study was to measure the relative change with metal loading in the number of reducible sites.

The XRD pattern of calcined 0.25 wt% $Pd/CeZrO_x$ (the predominant catalyst studied in this work) shows broad reflections at $2\theta = 29.2°$, 33.8°, 48.6° and 57.5°. This pattern (Fig. 3) is consistent mainly with the CeO_2 fluorite-cubic structure, as observed by other investigators [27,33,35]. All peaks in the pattern displayed a small shift to higher values of 2θ, as compared to fluorite cubic CeO_2 (JCPDS #43-1002), and this shift is associated with lattice contraction caused by the introduction of smaller Zr^{4+} ions in the CeO_2 lattice. No reflections corresponding to palladium or palladium oxide phases were detected, indicating the presence of small (<4 nm) particles.

The TPR profiles of calcined 0.25 wt% $Pd/CeZrO_x$ and $CeZrO_x$ are shown in Fig. 4. The profile of 0.25 wt% $Pd/CeZrO_x$ contains two reduction peaks: a sharp peak at 480 K and a broad peak centred at 720 K. The reduction profile of $CeZrO_x$ only displays a broad peak at 860 K. The 860 K reduction peak in the TPR of $CeZrO_x$ has been assigned to the reduction of surface Ce^{4+} [35]. The low temperature reduction peak in the TPR of $Pd/CeZrO_x$ has been assigned to the

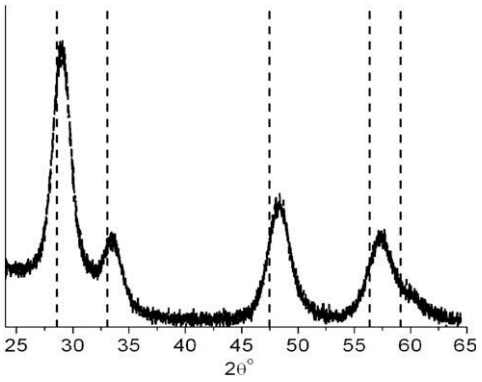

Fig. 3. XRD pattern of 0.25 wt% $Pd/CeZrO_x$. Dashed lines represent reflections from fluorite cubic phase of CeO_2.

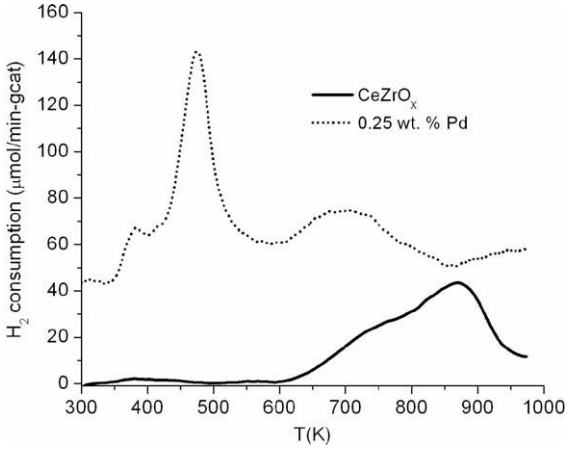

Fig. 4. TPR profiles of $CeZrO_x$ and 0.25 wt% $Pd/CeZrO_x$.

reduction of the metal, and of ceria species in intimate contact with the metal [27]. This interpretation is supported by hydrogen consumption measurements, which show that 10 times the amount of hydrogen is consumed for the 480 K reduction peak, than is required to reduce all the Pd^{2+} in the calcined catalyst to metallic Pd. The broad peak observed at 720 K for 0.25 wt% $Pd/CeZrO_x$ has been assigned to the reduction of surface ceria species that are not in contact with the metal [27], and this reduction is shifted to lower temperature (as compared to 860 K on the support alone) due to spillover of hydrogen from the metal. In summary, characterization results show that the $Pd/CeZrO_x$ catalysts used in this work consist of a reducible mixed oxide of Ce and Zr, containing both acidic and basic surface sites, and that the addition of Pd to $CeZrO_x$ promotes the reduction of ceria surface species in contact with Pd particles.

3.2. Reaction network

The conversion of 2-hexanone over 0.25 wt% $Pd/CeZrO_x$ was studied to probe the pathways for aldol condensation and related reactions catalyzed by metal, acidic and basic surface sites. The conversion of 2-hexanone was subsequently carried out at identical conditions on $CeZrO_x$ to address the effects of removing the metal sites for hydrogen dissociation. For brevity, the reaction products are grouped by carbon number, and the product distributions obtained at space velocities of 0.48 and 1.92 h^{-1} are summarized in Table 2. The temperature dependence of the product distributions resulting from 2-hexanone conversion over 0.25 wt% $PdCeZrO_x$ is shown in Table 3.

Table 2
Product distributions from the conversion of 2-hexanone over 0.25 wt% $PdCeZrO_x$ and $CeZrO_x$, at 623 K and 5 bar total pressure.

Catalyst	WHSV (h^{-1})	Conversion (%)	Carbon selectivities				
			C_{12} (%)	C_{18} (%)	C_{11} (%)	C_9 (%)	Alkanes ($\leqslant C_7$) (%)
0.25 wt% Pd $CeZrO_x$	1.92	58	83	2	2	5	8
0.25 wt% Pd $CeZrO_x$	0.48	77	69	3	3	11	13
$CeZrO_x$	1.92	21	66	25	–	7	2
$CeZrO_x$	0.48	33	46	31	–	18	5

Table 3
Effect of reaction temperature on the conversion of 2-hexanone over 0.25 wt% $Pd/CeZrO_x$ at 5 bar and WHSV = 1.92 h^{-1}.

T (K)	Conversion (%)	Carbon selectivities				
		C_{12} (%)	C_{18} (%)	C_{11} (%)	C_9 (%)	Alkanes ($\leqslant C_7$) (%)
573	42	96	1	1	1	1
598	49	93	1	1	2	2
623	60	83	2	2	5	8

The major organic liquid-phase product formed during the conversion of 2-hexanone over 0.25 wt% $Pd/CeZrO_x$ was the self-aldol condensation product, a C_{12} ketone (7-methyl-5-undecanone). Additionally, C_9 ketones ($m/z = 142$), C_{18} ketone ($m/z = 268$) and a C_{11} ketone (5-undecanone) were detected. Liquid-phase alkane products included hexane, with smaller amounts of 2-methyl-hexane and 5-methyl-undecane. Lighter alkanes (C_1–C_6) were detected in the gas phase, with methane, butane and hexane being the predominant gas phase species. As mentioned previously, 2-hexanone was observed to be in equilibrium with 2-hexanol, and a 9:1 ketone to alcohol ratio was measured experimentally at standard reaction conditions (5.5:1 H_2:2-hexanone ratio, 623 K, 5 bar). The experimentally measured ketone/alcohol ratio was consistent with the calculated ratio for the equilibrium conversion of acetone into 2-propanol at the aforementioned conditions.

The activity of $CeZrO_x$ towards 2-hexanone conversion was a factor of 3 lower than that of 0.25 wt% $Pd/CeZrO_x$ at 1.92 h^{-1} (Table 2). The major organic products formed in this conversion were unsaturated C_{12} ketones ($m/z = 182$), C_9 ketones, and a doubly unsaturated C_{18} ketone ($m/z = 264$). Additionally, significant amounts of C_{18} aromatic species (1,3,5-tributyl benzene and its isomers) were detected. Conversion to light alkane species was less than 5% at all reaction conditions.

The selectivities to C_9 and C_{18} species for both catalysts increased with decreasing space velocity, suggesting that these species are secondary reaction products resulting from further reactions of C_{12} ketones. Similarly, the selectivity towards light alkanes (on the Pd containing catalyst) increased by a factor of ~2 with decreasing space velocity. The combined selectivities to C_9 and C_{18} products also decreased with decreasing reaction temperature, and decreased by a factor of ~3 at 0.48 h^{-1} when adding Pd to $CeZrO_x$ to form the 0.25 wt% $PdCeZrO_x$ catalyst.

A reaction network is presented in Fig. 5 for $Pd/CeZrO_x$, based on the observed product distributions and results from studies of acetone condensation [36,37]. Species marked with an asterisk are reaction intermediates that were not detected in the reaction effluent. These intermediates are believed to react rapidly, leading to undetectable steady-state concentrations. The primary reaction pathway involves the self-coupling of 2-hexanone (0) to yield 7-methyl-5-undecanone (3). In this pathway, 2-hexanone undergoes self-aldol condensation on basic sites to form an aldol alcohol (1), which then undergoes dehydration on acidic (or basic) sites to form an α–β unsaturated ketone (2), followed by hydrogenation on metal sites to yield a saturated ketone (3). Neither the aldol alcohol nor the α–β unsaturated ketone was observed in the reaction effluent, suggesting that the dehydration and hydrogenation reactions are fast in comparison to aldol condensation. 7-methyl-5-undecanone undergoes further aldol condensation with 2-hexanone (in the pathway described above) to yield a C_{18} ketone (4). Similar observations were reported by Di Cosimo for the self-coupling of 2-propanol on $Cu/MgAlO_x$ [21].

Thermodynamic analysis shows that C–C coupling steps involving aldol condensation and dehydration are equilibrium limited (such as (0) → (2)). In contrast, the hydrogenation of α–β unsaturated ketones such as (2) is not equilibrium limited at these conditions [5,23]. This hydrogenation reaction prevents reverse-aldol reactions, and therefore drives C–C coupling reactions towards higher conversions. Therefore, the absence of a hydrogenation functionality on $CeZrO_x$ limits the yields of C_{12} condensation products.

The equilibrated hydrogenation of the C═O group of 2-hexanone yields 2-hexanol, which can undergo dehydration over acidic sites to yield hexene. Hexene is not observed among the reaction products, because it is rapidly hydrogenated to form hexane. By analogy, 7-methyl-5-undecanone undergoes dehydration and hydrogenation steps to form 5-methyl undecane (7). Alcohols have been shown to undergo reforming (cleavage of C–C bonds adjacent to the –COH group) over metal catalysts to yield CO_x species and alkanes. In this respect, 2-hexanol undergoes reforming to form methane, butane and CO_x [38,39]. As we will show in subsequent sections, CO_x species are hydrogenated to methane over 0.25 wt% $Pd/CeZrO_x$, and only small amounts of CO_x species (<1% of total carbon) are detected in the gas phase. Similarly, 7-methyl-5-undecanol (5) undergoes reforming to yield methane and 2-methyl hexane (6). These reforming and dehydration steps remove the C═O functionality, and they are therefore detrimental to C–C coupling processes.

The reaction temperature was varied to determine the apparent activation energies of reactions forming the C_{12}, C_{18} and C_9 species resulting from the conversion of 2-hexanone over 0.25 wt% $Pd/CeZrO_x$. The apparent activation energies were calculated from Arrhenius plots in Fig. 6. The apparent activation energy for C_{12} formation was found to be 15 kJ/mol, in agreement with the value obtained by Al-Wadaani et al. [40] for the conversion of acetone to MIBK over $Pd/ZnCrO_x$, a similar reducible amphoteric oxide. The apparent activation energy of C_{18} formation (28 kJ/mol) was comparable to that of C_{12} formation, suggesting that both species form through similar bond-making processes (aldol condensation). In contrast, the apparent activation energy for the formation of C_9 species is an order of magnitude higher (140 kJ/mol). The C_9 ketones could not have been formed by aldol condensation, because this process would yield oligomers with carbon numbers that are

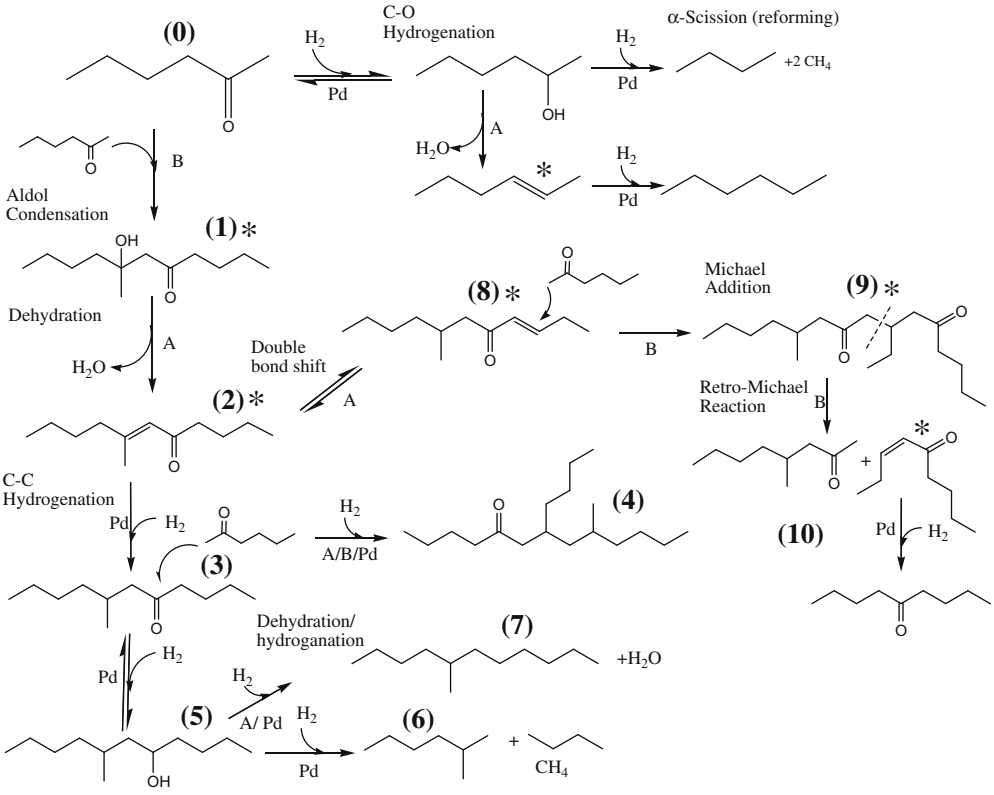

Fig. 5. Proposed reaction scheme for the conversion of 2-hexanone on Pd/$CeZrO_X$. The numbers in parentheses are referenced in the text. A, B and Pd refer to acidic, basic and palladium sites, respectively. * represents reaction intermediates not observed in effluent.

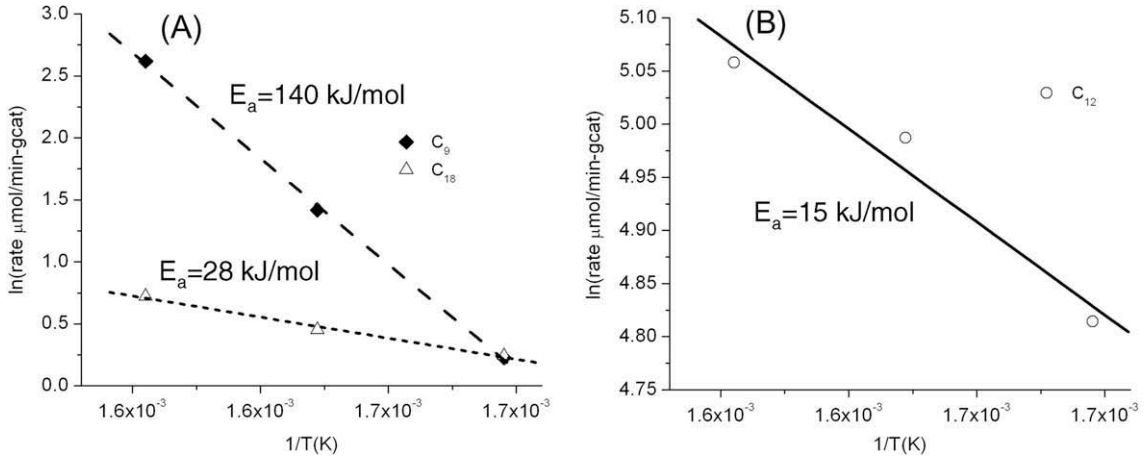

Fig. 6. Arrhenius plots and calculated activation energies for the formation of C_9 and C_{18} species (A) and C_{12} species (B) from the conversion of 2-hexanone on 0.25 wt% Pd/$CeZrO_x$.

multiples of six. The high apparent activation energy associated with C_9 formation suggests that a bond-breaking step decreases the carbon number in the products. Furthermore, the absence of significant amounts of C_3 species suggests that the C_9 products are not formed via degradation of C_{12} ketones, and that the cleavage of C_{18} products may be involved.

One possible pathway for the formation of C_9 ketones proceeds through C=C double bond migration in the α–β unsaturated aldol product (2) followed by Michael addition with 2-hexanone on basic catalytic sites to produce a C_{18} dione (9). Migration of the C=C double bond in α–β unsaturated ketones has been observed by Mussolino et al. over Pd/TiO_2 [41]. The conversion of 2-butanone over $CeZrO_x$ in the present study showed the existence of double bond migration, because α–β unsaturated condensation products (C_8 ketones) with the C=C double bond in different positions were identified by GC/MS analysis. These products included 5-methyl-4-hepten-3-one, 5-methyl-5-hepten-3-one and 5-methylene-3-heptanone. The resulting unsaturated ketone (8) contains a less substituted double bond, which is more susceptible to Michael addition with 2-hexanone to form a dione (9). The C_{18} dione then undergoes retro-Michael reaction [42] to form the two different C_9 ketones (10) identified in the effluent. Finally, small amounts (~2% selectiv-

ity) of a C_{11} ketone (5-undecanone) may be obtained from C–C hydrogenolysis of the methyl branch of 7-methyl-5-undecanone, also yielding methane (not shown in the figure).

Reactions involving α–β unsaturated ketones become more significant over $CeZrO_x$, because these species are not stabilized against further reaction by hydrogenation. The selectivity towards C_9 and C_{18} secondary products is enhanced substantially compared to that on 0.25 wt% PdCeZrOx. Furthermore, the α–β unsaturated ketone (2) can undergo cross-aldol condensation with 2-hexanone followed by a 1,6-aldol addition or aromatization to form 1,3,5-tributylbenzene, a C_{18} species. This reaction is analgous to the formation of mesitylene from acetone [36,37]. It is also important to note that C=O hydrogenation (that produces alcohols), reforming, and hydrogenolysis reactions are minimized in the absence of Pd.

3.3. Effects of partial and total pressures.

Reaction kinetic studies were conducted to determine the reaction orders with respect to 2-hexanone and H_2. These studies were performed using an inert species (heptane for 2-hexanone, He for H_2) to change the partial pressures of 2-hexanone and hydrogen independently, while maintaining the total pressure constant. The space velocity of the reaction system was adjusted to achieve conversions of <30%. At these conversions, secondary products were produced in negligible yields. The logarithm of the reaction rate (μmol C_{12} min^{-1} g cat^{-1}) was plotted against the logarithm of the partial pressure of the species, with the slopes yielding the reaction orders, as shown in Fig. 7. For both hydrogen and 2-hexanone, the reaction orders were fractional and decreased with increasing partial pressures. For 2-hexanone, the reaction order was 0.9 for low partial pressures (0.08–0.16 bar), whereas it decreased to 0.5 as partial pressure was increased (0.31–0.63 bar). For hydrogen, the order decreased from 0.8 to 0.6 going from low to higher partial pressures (0.9–3.5 bar).

Several investigators have studied the aldol condensation of acetone with citral on basic oxides. Diez et al. showed that the rate-determining step in the reaction is the abstraction of an α-hydrogen from acetone over a Li-doped MgO catalyst [43]. However, Abello et al. showed the slow step to be the surface reaction in which the enolate ion generated from an acetone molecule attacks a citral molecule over $MgAlO_x$ [44]. Either rate-determining step is possible for 2-hexanone self-condensation. If it is abstraction of an α-hydrogen atom, then the reaction order with respect to 2-hexanone in the numerator of a Langmuir–Hinshelwood type rate expression should be 1, and if the rate-determining step is the surface reaction, the reaction order in the numerator would be 2. However, under the partial pressures used here, inhibition due to surface coverage by reactant or product species reduces the apparent reaction order, as observed by both previous investigators, and it is possible that either first-order or second-order kinetics is approached in the limit of low 2-hexanone partial pressures. The apparent reaction orders for 2-hexanone conversion observed in the present study are similar to ones found by Torres et al. and Melo et al. for acetone condensation reaction. [10,45] Torres et al. calculated an apparent order in 2-propanol of 0.35 for the MIBK formation rate for partial pressures of 2-propanol around 0.4 bar. Melo et al. found that the apparent order with respect to acetone was 0.3. Also Melo et al. reported an apparent reaction order in hydrogen of 1.3 for partial pressures up to 0.8 bar, which is in accordance with the values found in the present study for a higher partial pressure range. The effects of total reactor pressure on the condensation activity and selectivity are shown in Table 4. The conversion of 2-hexanone is increased significantly upon increasing the total pressure, while the selectivity to primary and secondary products remained approximately constant. This behavior results from a combination of the effects of increasing H_2 and 2-hexanone partial pressures that were documented above.

3.4. Effect of metal loading and metal-support proximity

The activity and selectivity data for the conversion of 2-hexanone over $Pd/CeZrO_x$ catalysts with different metal loadings are given in Table 5. The selectivity towards saturated C_{12} product decreases with increasing metal loadings. The decline in selectivity towards the major condensation product is accompanied by an increase in selectivity towards light alkanes. This result demonstrates that higher metal loadings promote hydrogenolysis reactions to form hexane and reforming reactions leading to the formation of butane and methane. These reactions take place in parallel with the condensation reaction pathway leading to the C_{12} ketone. It is important to note that hydrogenation of the α–β unsaturated ketone is complete for all metal loadings, as unsaturated C_{12} species were not detected in the effluent. This observation shows that the hydrogenation step of the overall ketone coupling process is a fast step in the reaction network. Therefore, the rates of the side reactions, such as hydrogenolysis and reforming, can be minimized by avoiding the use of excess metal functionality.

The importance of the proximity of metal sites to acid/base sites was investigated by comparing the conversion of 2-hexanone over

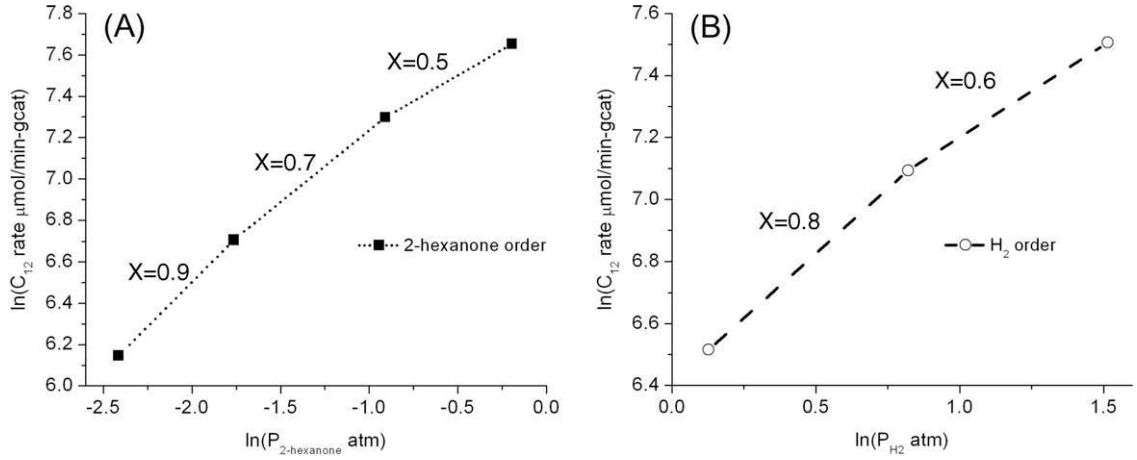

Fig. 7. Rate versus partial pressure, and calculated reaction orders with respect to 2-hexanone pressure at P_{H2} = 4.2 bar (A) and with respect to hydrogen pressure at $P_{2-hexanone}$ = 0.8 bar (B).

Table 4
Effect of total pressure on the conversion of 2-hexanone over 0.25 wt% Pd/$CeZrO_x$ at 623 K and WHSV = 1.92 h^{-1}.

P_{total} (bar)	Conversion (%)	Carbon selectivities				
		C_{12} (%)	C_{18} (%)	C_{11} (%)	C_9 (%)	Alkanes ($\leqslant C_7$) (%)
5	58	83	2	2	5	8
16	75	80	3	2	4	10
25	84	79	5	2	4	9

Table 5
Product distributions from conversion of 2-hexanone over Pd/$CeZrO_x$ with different metal loadings, and a physical mixture of 0.5 wt% Pd/SiO_2 and $CeZrO_x$ at 623 K and 5 bar total pressure.

Catalyst	WHSV (h^{-1})	Conversion (%)	Carbon selectivities				
			C_{12} (%)	C_{18} (%)	C_{11} (%)	C_9 (%)	Alkanes ($\leqslant C_7$) (%)
0.05 wt% Pd/$CeZrO_x$	1.92	68	85	3	2	4	3
0.25 wt% Pd/$CeZrO_x$	1.92	58	83	2	2	5	8
1.45 wt% Pd/$CeZrO_x$	1.92	85	57	2	1	4	36
0.5 wt% Pd/SiO_2	2.84	6	12	–	–	–	87
0.5 wt% Pd/SiO_2 + $CeZrO_x$	1.92*	48	77	10	4	5	3

a physical mixture of Pd/SiO_2 and $CeZrO_x$ to that over 0.25 wt% Pd/$CeZrO_x$, and the results are presented in Table 5. Due to the weak acid/base properties of Si–OH groups on the surface, the SiO_2 support can be considered to be inert [5]. In this respect, 0.5 wt% Pd/SiO_2 was tested alone, and a very low conversion of 2-hexanone (6%) was observed, with a low selectivity towards the C_{12} ketone (12%). A physical mixture of 0.5 wt% Pd/SiO_2 with $CeZrO_x$ was then prepared to give the same amount of acid, base and metal functionality as 0.25 wt% Pd/$CeZrO_x$, and this physical mixture was studied for 2-hexanone condensation at the same reaction conditions. A lower (~10%) activity was obtained in the case of the physical mixture. Even though the selectivity towards the C_{12} ketone did not vary considerably from that on 0.25 wt% Pd/$CeZrO_x$, the selectivity towards higher molecular weight products, such as C_{18} aromatics was increased at the expense of light alkanes on the physical mixture. This change in selectivity suggests that a metal-support interaction is responsible for reforming reactions and dehydration/hydrogenation reactions. In addition, because the α–β unsaturated aldol condensation product cannot be hydrogenated on the physical mixture unless it desorbs from the $CeZrO_x$ surface, it has a higher probability to undergo further condensation reactions (e.g., Michael or aldol) to produce the higher molecular weight species using the pathways described earlier.

3.5. Effects of oxygenated additives and water

The influence of oxygenated compounds such as primary alcohols, secondary alcohols, 3-ketones, heterocyclics and carboxylic acids on the aldol condensation of ketones was studied, because these species represent classes of compounds (together with 2-ketones) present in the hydrophobic organic mixture derived from the conversion of sugars or polyols over a Pt–Re/C catalyst [4]. One representative species was selected from each group to facilitate the analysis, and the results are given in Table 6. An experiment with 10 mol% inert species (heptane) serves as a benchmark for the additives study (entry 2), because although heptane is expected to be inert, it may act as a diluent and therefore decrease the overall rate of a positive order reaction. Results (entry 2) show that heptane has little effect on the activity and selectivity of 2-hexanone conversion.

The effect of a primary alcohol on the self-condensation of 2-hexanone was studied by feeding a mixture of 10 mol% 1-butanol in 2-hexanone (entry 3). At the reaction conditions used in this study, primary alcohols are readily equilibrated (through dehydrogenation) with the corresponding aldehydes, in this case butanal [46]. The aldehydes can undergo self-aldol condensation reactions or cross-aldol condensation reactions with ketones, where the ketones act as the nucleophilic species. A reaction scheme for the conversion of primary alcohols is illustrated in Fig. 8A. Condensation of butanal with 2-hexanone yields 5-decanone, and this product accounted for 26% of the product carbon. The self-condensation product of butanal, 2-ethyl hexanal, was not observed due to the low concentration of butanal. Butanal can also undergo decarbonylation reaction to produce CO and propane [47], which were both detected in the effluent. A significant decrease in the activity of 2-hexanone self-condensation (70%) was caused by the addition of the primary alcohol, which was almost completely converted. This loss of activity was completely reversed upon a 12 h treatment in flowing H_2 and removal of the primary alcohol from the feed. Possible causes for inhibition by primary alcohols include strongly bound aldehyde species [33] or oligomers of butanal that can act as coke precursors [48,49] and which can be removed by H_2 treatment. Microcalorimetric studies have shown that primary alcohols and aldehydes bind more strongly to metal and basic sites compared to secondary alcohols and ketones [50,51]. Therefore, it is likely that the catalytic sites required for coupling of ketones are preferentially occupied by primary alcohols or aldehydes under reaction conditions, leading to inhibition of ketone coupling. Lowering the WHSV to 0.48 h^{-1} increased 2-hexanone conversion to 65% and the C_{12} selectivity to 60%, showing that the detrimental effect of primary alcohols on condensation activity can be overcome if the inhibiting species are reacted to completion.

The effect of secondary alcohols on the self-condensation of 2-hexanone was studied by feeding a mixture of 10 mol% 2-butanol in 2-hexanone (entry 4). Secondary alcohols are dehydrogenated to quasi-equilibrium with the corresponding ketones (2-butanone in this case), the latter of which can undergo either self- or cross-condensation, as illustrated in Fig. 8B The observed products are the self-condensation product of 2-hexanone and the cross-condensation product of 2-butanone and 2-hexanone (3-methyl-5-nonanone and/or 5-methyl-3-nonanone). If α-hydrogen atoms of the methyl group are abstracted from 2-butanone, and the resulting carbanion attacks the carbonyl group of 2-hexanone, then 3-methyl-5-nonanone is formed. In the opposite case, 5-methly-3-pentanone is formed. The 2-butanone self-condensation product was not observed due to the low 2-butanone concentration, result-

Table 6
Effects of monofunctional oxygenates and water on the conversion of 2-hexanone and 2-butanone over 0. 25 wt% Pd/$CeZrO_x$ at 623 K, 5 bar and WHSV = 1.92 h^{-1}.

Entry	Feed (mol%)	Conversion		Primary product(s)		Secondary product(s)	
		Ketone (%)	Additive (%)	Species	Selectivity (%)	Species	Selectivity (%)
1	2-Hexanone	58	–	7-Methyl-5-undecanone (C_{12} ketone)	83	C_{18} ketones C_9 ketones Alkanes ($\leqslant C_7$) C_{11} ketones	2 5 8 2
2	90% 2-Hexanone and 10% heptane	56	0	7-Methyl-5-undecanone (C_{12} ketone)	75	C_{18} ketones C_9 ketones Alkanes ($\leqslant C_7$) C_{11} ketones	1 6 14 4
3	90% 2-Hexanone and 10% 1-butanol	29	100	7-Methyl-5-undecanone (C_{12} ketone) 5-Decanone (C_{10} ketone)	47 26	C_{18} ketones C_9 ketones Alkanes ($\leqslant C_7$) C_{11} ketones $CO + CO_2$	1 4 17 3 1
4	90% 2-Hexanone and 10% 2-butanol	53	65	7-Methyl-5-undecanone (C_{12} ketone) 3-Methyl-5-nonanone and 5-methyl-3-nonanone (C_{10} ketones)	77 11	C_{18} ketones C_9 ketones Alkanes ($\leqslant C_7$) C_{11} ketones	2 4 4 2
5	90% 2-Hexanone and 10% butanoic acid	8	100	7-Methyl-5-undecanone (C_{12} ketone) 4-Heptanone (C_7 ketone) 5-Decanone (C_{10} ketone)	35 28 2	C_{18} ketones C_9 ketones Alkanes ($\leqslant C_7$) C_{11} ketones $CO + CO_2$	0 6 24 4 1
6	90% 2-Hexanone and 10% THF	48	12	7-Methyl-5-undecanone (C_{12} ketone)	72	C_{18} ketones C_9 ketones Alkanes ($\leqslant C_7$) C_{11} ketones	1 7 16 5
7	75% 2-Hexanone and 25% 3-pentanone	50	27	7-Methyl-5-undecanone (C_{12} ketone) 7-Ethyl-5-nonanone (C_{11} ketone)	73 9	C_{18} ketones C_9 ketones Alkanes ($\leqslant C_7$) 5-Undecanone	1 5 9 3
8	2-Butanone	70	–	5-Methyl-3-heptanone	91	C_6 ketones C_{12} ketones Alkanes ($\leqslant C_7$)	2 5 2
9	Water-saturated 2-butanone (12 wt% water)	39	–	5-Methyl-3-heptanone	93	C_6 ketones C_{12} ketones Alkanes ($\leqslant C_7$)	1 3 3

ing in preferential cross-condensation. The overall ketone conversion was 55%, showing that secondary alcohols do not significantly affect the condensation activity.

The effect of carboxylic acids was investigated using a 10 mol% butyric acid in 2-hexanone feed (entry 5). The butyric acid was found to ketonize to 4-heptanone and also undergo a coupling reaction with 2-hexanone to form 5-decanone. The 5-decanone results from the aldol condensation of 2-hexanone with butanal, which is formed upon the partial reduction of butanoic acid. The reactions involved in the conversion of butanoic acid are illustrated in Fig. 8C. The addition of acid causes a significant loss in activity for 2-hexanone self-condensation, such that the 2-hexanone conversion decreased from 58% to 8%. However, complete deactivation was not observed and the activity could be regained as described for primary alcohols. Poisoning of the basic catalytic sites by carboxylic acids is the most probable cause for the loss of activity [49,52]. Further poisoning of the basic sites may be caused by the CO_2 released from the ketonization reaction of butyric acid. The effect of CO_2 was investigated separately and will be explained in the following sections. Decreasing the space velocity to 0.48 h^{-1} increased the 2-hexanone conversion and C_{12} selectivity to 48% and 56%, respectively. It should be noted that selectivities to light alkanes are substantially higher in the presence of either primary alcohols or carboxylic acids as compared to secondary alcohols or ketones. The production of additional alkanes results from the more facile reforming of the terminal functionalized carbon in comparison to internal C–C cleavage.

A slight decrease of 2-hexanone self-condensation activity resulted with the addition of 10 mol% THF (2-hexanone conversion declined from 58% to 48%, entry 6). Product analysis revealed that 10% of the THF was converted, and the amount of propane detected approximately matched the amount of THF converted. This result suggests a ring opening reaction yielding a linear oxygenated intermediate species, 1-butanol, which undergoes further decarbonylation to produce propane as observed by Kreuzer et al. [47]. Therefore, the decrease of activity can be attributed to partial conversion of THF to 1-butanol, for which the deactivating effects of primary alcohols were explained above.

The effect of 3-ketones was investigated (entry 7) via the reaction of a 25 mol% mixture of 3-pentanone in 2-hexanone. The self-condensation of 3-pentanone was not observed, and the cross-condensation of 3-pentanone with 2-hexanone was slower relative to the self-condensation of 2-hexanone. The methyl group in 2-ketones contains α-hydrogen atoms that upon abstraction lead to a more stable carbanion, than the secondary carbanions that form upon abstraction of α-hydrogen atoms from 3-ketones. Furthermore, the methyl carbanion is less sterically hindered than internal carbanions. The aforementioned properties make the methyl

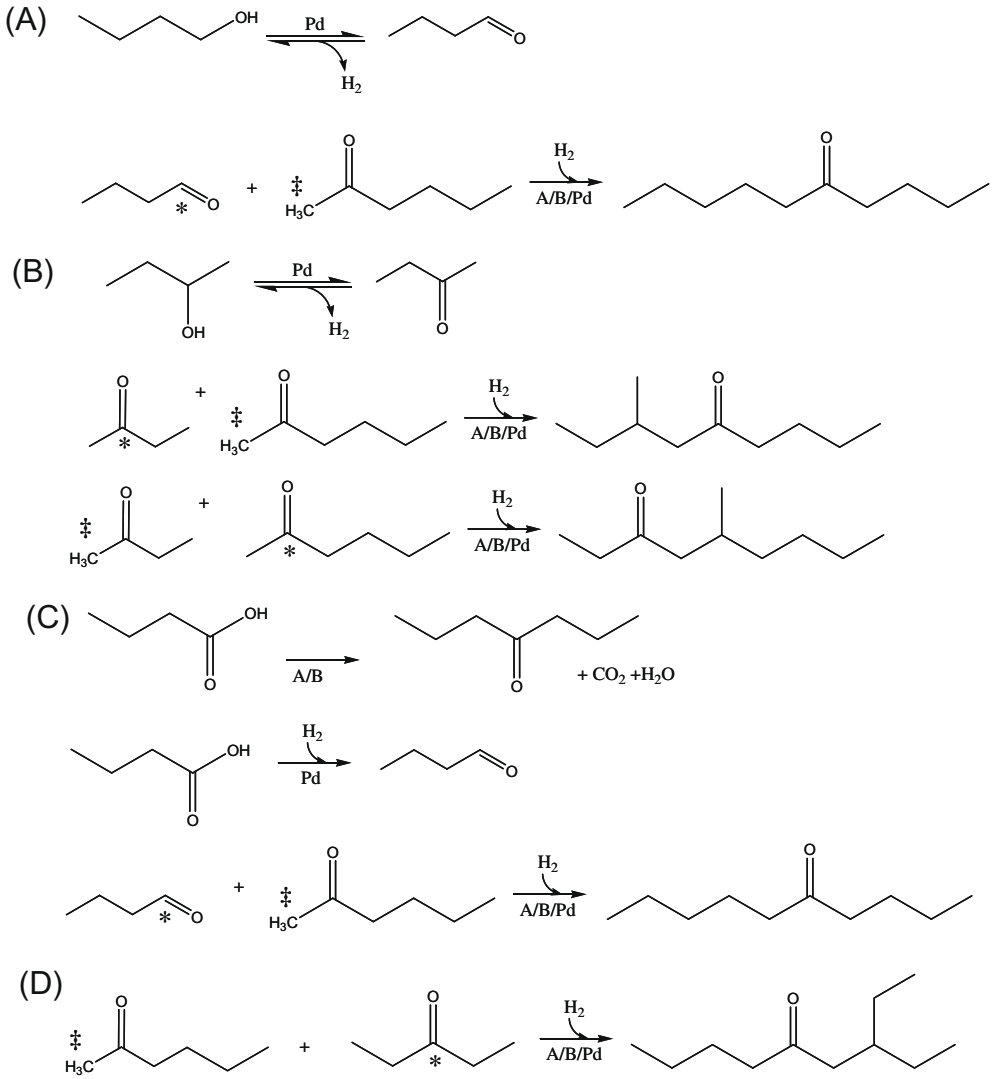

Fig. 8. Reactions of selected oxygenates-primary alcohols (A), secondary alcohols (B), carboxylic acids (C) and 3-ketones (D). For aldol-type reactions, the source of the carbanion is indicated by ‡, and the attacked carbonyl group is indicated by ⁎.

carbanion a better nucleophile than secondary carbanions. Additionally, the carbonyl group of 3-ketones is more sterically hindered than that of 2-ketones, making it less susceptible to nucleophilic attack [53]. In this respect, the self-condensation of 2-hexanone is favoured over cross-condensation with 3-pentanone, which is favoured substantially over the self-condensation of 3-pentanone. Accordingly, a single cross-condensation product (where 2-hexanone acts as the nucleophile) would be expected, as illustrated in Fig. 8D. These results are observed experimentally.

In addition to containing alkanes and oxygenated hydrocarbon species, organic streams derived from the conversion of sugars over Pt–Re/C are saturated with water, resulting from contact with an aqueous phase. Water is also formed as a by-product of aldol condensation, and associated secondary hydrogenolysis reactions. Furthermore, water is produced during ketonization. Accordingly, it is important to study the effects of water on the self-coupling of ketones, and in this respect we have investigated the effects of water on the self-aldol condensation of 2-butanone into 5-methyl-2-heptanone (Entries 8 and 9). In these studies, 2-butanone was chosen as the reactant, because it can be saturated with a larger amount of water (∼12 wt%) than 2-hexanone, and this water content is representative of the products of ketonization. The addition of water decreased the condensation activity by 40%, and this activity loss was reversible, suggesting inhibition.

The inhibition of the aldol condensation activity by water may be responsible for the fractional H_2 and 2-hexanone reaction orders described previously. In this respect, Gammara et al. report that the presence of relatively large amounts of molecularly adsorbed water on ceria is responsible for inhibition of CO oxidation on Cu/CeO_x catalysts [54]. Moreover, Gutierrez-Ortiz et al. showed by H_2O–TPD experiments that the hydrophilicity of ceria is increased by addition of ZrO_2 [55]. In addition to inhibition by site blocking, the presence of water may also shift the aldol condensation equilibrium to the reactants side by inhibiting dehydration of the aldol-alcohol product.

3.6. Effect of CO_2 co-feeding

Carbon dioxide is produced as a by-product of the ketonization of carboxylic acids. Therefore, it is necessary to understand the effects of the by-product CO_2 on the self-coupling of ketones to accomplish the integration of ketonization and aldol condensation/hydrogenation in a single reactor system. To that end, we have substituted the pure hydrogen gas co-feed used above with H_2–CO_2

Table 7
Effects of CO_2 on the conversion of 2-hexanone on $CeZrO_x$ and $Pd/CeZrO_x$ at 623 K and 5 bar total pressure.

Catalyst	% CO_2 in H_2	WHSV (h^{-1})	Conversion		Carbon selectivities				
			Ketone (%)	CO_2 (%)	C_{12} (%)	C_{18} (%)	C_{11} (%)	C_9 (%)	Alkanes (C_2–C_7) (%)
0.25 wt% Pd $CeZrO_x$	10	1.92	5	63	22	0	5	18	55
0.25 wt% Pd $CeZrO_x$	10	0.48	17	45	12	–	4	24	60
0.25 wt% Pd $CeZrO_x$	5	1.92	7	44	26	0	7	26	41
$CeZrO_x$	10	1.92	7	0	45	4	–	46	5

gas mixtures. The results of CO_2 co-feeding at various conditions are shown in Table 7. Co-feeding a 10 mol% CO_2 in H_2 stream resulted in almost complete loss of self-condensation activity on 0.25 wt% Pd/$CeZrO_x$, decreasing the conversion of 2-hexanone from 60% to 5%. Under these conditions, 63% of the CO_2 was converted to CO by the reverse water–gas shift reaction and to CH_4 by methanation, and 2-hexanone was observed to be in equilibrium with 2-hexanol. Carbon monoxide adsorbs more strongly than hydrogen on the Pd surface, and CO poisoning has been reported in hydrogenation reactions [56,57]. However, the observation of quasi-equilibration of 2-hexanone with 2-hexanol in the presence of CO (derived from reduction of CO_2) suggests that hydrogenation is still fast in the presence of CO, possibly because of the high reaction temperatures.

A decrease in the concentration of CO_2 in the co-feed to 5% did not improve the self-coupling yield. Similarly, decreasing the space velocity of the ketone feed was not effective in overcoming the effects of CO_2. The self-coupling of 2-hexanone was also significantly suppressed on $CeZrO_x$, suggesting that CO_2 influences aldol condensation sites on the support. For all conditions listed in Table 7, the activity loss associated with CO_2 was observed to be completely reversible upon removal of CO_2 from the gas co-feed stream. Kamimura et al. showed that co-feeding of CO_2 suppresses the aldol condensation activity of $CeFeO_x$ catalysts, and they attribute this effect to the blocking of basic catalytic sites by acidic CO_2 [58]. The suppression of basic catalytic sites by CO_2 causes the product selectivity to be substantially altered by reactions taking place on other functionalities such as metal and acidic sites, thereby leading to higher selectivities to alkanes for all conditions in Table 7. The alkanes are formed by dehydration/hydrogenation, and reforming of 2-hexanol.

3.7. Interaction of CO_2 with $Pd/CeZrO_x$ and $CeZrO_x$

The carbon dioxide desorption profiles described in Section 3.1 show that CO_2 desorption from $Pd/CeZrO_x$ persists at temperatures up to 1000 K. It is therefore, interesting to note that the loss of activity resulting from CO_2 co-feeding was completely reversible on 0.25 wt% $Pd/CeZrO_x$ and $CeZrO_x$ at a temperature of 623 K, because a fraction of the adsorbed CO_2 may still be blocking active basic sites, even after desorption at this reaction temperature. Due to the setup of our reactor system we were not able to obtain a transient reaction profile needed to establish the relationship between the rate of CO_2 desorption at 623 K and the return of aldol condensation activity; however, activity was returned after 6–12 h treatment in H_2 at reaction temperature.

Strongly binding sites may become irreversibly covered by tightly bound spectator species that prevent catalytic turnover. Since these sites do not participate in the overall reaction, their deactivation by CO_2 will not be reflected in catalytic activity measurements. However, the catalyst regeneration studies carried out in the present work employed flowing H_2, whereas CO_2-TPD studies were carried out using an inert carrier gas. Therefore, studies employing TPSR of CO_2 under flowing H_2 were carried out. Fig. 9 shows the desorption profiles of CO_2 and associated products (CO and methane) for 0.25 wt% $Pd/CeZrO_x$ and $CeZrO_x$. On 0.25 wt% $Pd/CeZrO_x$, the desorption of CO_2 was complete by 620 K, and was accompanied by the production of CO and methane, which peaked at 550 and 650 K, respectively. Palladium is a poor catalyst for the methanation of CO_2 and CO [59]. However, the presence of a reducible support such as CeO_2 has been shown to substantially promote the activity of Pd for CO_2 activation. Leitenberg et al. propose a mechanism in which Ce^{4+} is reduced to Ce^{3+} by hydrogen, which is activated via dissociation over a metal, followed by spillover onto the support [60]. The resulting Ce^{3+} reacts with CO_2 to form CO and regenerates Ce^{4+}. The formation of Ce^{3+} is required for the activation of CO_2. In agreement with this behavior, we observe that the onset temperature of CO formation (450 K) in TPSR corresponds to the reduction temperature (obtained from TPR) of Ce^{4+} in intimate contact with Pd. At higher temperatures (>600 K), CO is hydrogenated to methane. Accordingly, the activation of CO_2 by a hydrogen-reduced ceria permits the removal of CO_2 from the surface at substantially lower temperatures than in the absence of hydrogen.

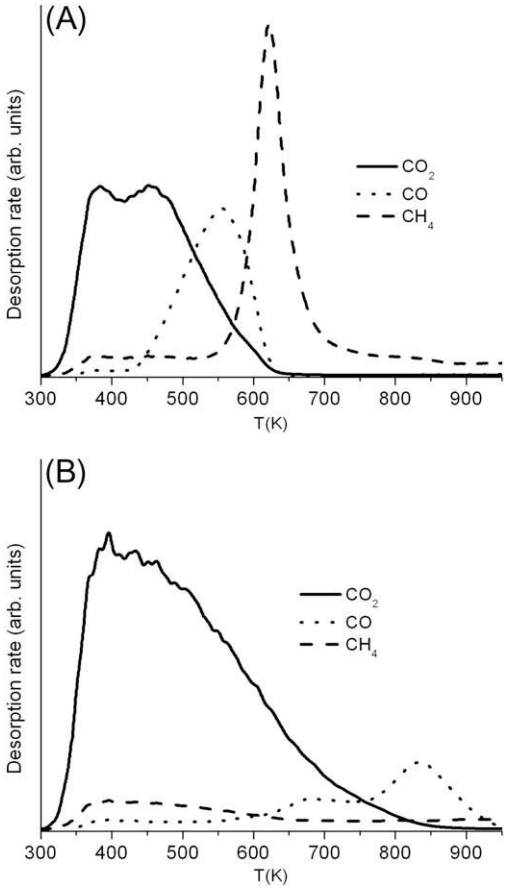

Fig. 9. TPSR of adsorbed CO_2 under H_2 for 0.25 wt% $Pd/CeZrO_x$ (A) and $CeZrO_x$ (B).

Fig. 9B shows that even in the absence of metal, desorption of CO_2 from $CeZrO_x$ is facilitated by the presence of hydrogen, with CO_2 desorbing completely at 850 K. This observation may explain the fact that even $CeZrO_x$ regains catalytic activity after regeneration with hydrogen, and suggests that hydrogen interacts with the surface in the absence of a metal. In this respect, Kondo et al. have observed the dissociation of hydrogen on ZrO_2 to form Zr–OH surface species at temperatures above 373 K[61]. These species may drive the conversion of surface carbonates into more labile species, thereby facilitating the desorption of CO_2. Furthermore, the desorption of CO_2 above ~700 K is accompanied by the production of CO, which subsides at a temperature near 900 K. As with the presence of metal, the production of CO appears to be associated with the reduction of surface CeO_2 species observed in TPR.

4. Conclusions

The self-coupling of 2-hexanone to form C_{12} species via aldol condensation/hydrogenation was studied over $Pd/CeZrO_x$ catalysts. XRD studies show that the $CeZrO_x$ support consists of a cerium–zirconium solid solution. TPR studies of these catalysts indicate that the presence of palladium causes reduction of neighbouring ceria species. Ammonia and CO_2 TPD profiles indicate the presence of both acidic and basic functionalities. TPSR studies in flowing H_2 for catalysts containing adsorbed CO_2 indicate that CO_2 is converted to CO over Ce^{3+} sites that are formed during reduction of Ce^{4+} to Ce^{3+}. Reaction kinetics studies show that the primary product of aldol condensation/hydrogenation is C_{12} ketone, with the formation of C_9 and C_{18} ketones as secondary products, as well as the production of light alkanes (C_1–C_7). The high activation energy of C_9 formation (140 kJ/mol) compared to the formation of C_{12} and C_{18} species (15 and 28 kJ/mol, respectively), and the increase in the selectivity towards C_9 species in the absence of Pd, indicate that these species may be formed as a result of the decomposition of unsaturated C_{18} condensation products. The light alkane species are formed as a result of dehydration/hydrogenation and reforming of 2-hexanol. The self-coupling of 2-hexanone was found to be positive order in both 2-hexanone and hydrogen, and consequently the yield to C_{12} products was found to increase with total reaction pressure. Lower metal loadings resulted in enhanced selectivity to C_{12} products and suppressed de-oxygenation side reactions. Metal-support proximity was not found to substantially influence catalyst performance, although it had a measureable effect on the formation of secondary products.

Monofunctional oxygenated additives such as primary alcohols and carboxylic acids were found to reversibly inhibit the self-coupling activity of 2-hexanone. The detrimental effects of these species could be overcome by increasing the overall reaction residence time. Water (the product of both aldol condensation and ketonization) and carbon dioxide (a product of ketonization) were also observed to reversibly inhibit 2-hexanone self-coupling. These observations lead us to conclude that it may be difficult to integrate efficiently the ketonization of carboxylic acids and the aldol condensation/hydrogenation of ketones in a single reactor system. However, because water and CO_2 can easily be separated from the organic reaction mixture, the operation of a cascade system consisting of separate ketonization and aldol condensation reactors appears to be preferred.

Acknowledgments

This work was supported by the US Department of Energy Office of Basic Energy Sciences, and the Great Lakes Bioenergy Research Centre (GLBRC) funded by DOE at the University of Wisconsin. We also thank Professor Manos Mavrikakis for valuable discussions and collaborations throughout this project.

References

[1] Annual Energy Outlook 2009, Energy Information Administration of the US Department of Energy, March 2009.
[2] J.A. Kinast, Production of Biodiesels from Multiple Feedstocks and Properties of Biodiesels and Biodiesel/Diesel Blends, National Renewable Energy Laboratory, 2003.
[3] B. West, K. Knoll, W. Clark, R. Graves, J. Orban, S. Przesmitzki, T. Theiss, Effects of Intermediate Ethanol Blends on Legacy Vehicles and Small Non-Road Engines, National Renewable Energy Laboratory, 2008.
[4] E.L. Kunkes, D.A. Simonetti, R.M. West, J.C. Serrano-Ruiz, C.A. Gärtner, J.A. Dumesic, Science 322 (2008) 417.
[5] A.A. Nikolopoulos, B.W.L. Jang, J.J. Spivey, Appl. Catal. A 296 (2005) 128.
[6] O. Nagashima, S. Sato, R. Takahashi, T. Sodesawa, J. Mol. Catal. A 227 (2005) 231.
[7] R.M. West, Z.Y. Liu, M. Peter, J.A. Dumesic, ChemSusChem 1 (2008) 417.
[8] K.M. Dooley, A.K. Bhat, C.P. Plaisance, A.D. Roy, Appl. Catal. A 320 (2007) 122.
[9] M. Glinski, J. Kijenski, A. Jakubowski, Appl. Catal. A 128 (1995) 209.
[10] G. Torres, C.R. Apesteguia, J.I. Di Cosimo, Appl. Catal. A 317 (2007) 161.
[11] K.H. Lin, A.N. Ko, Appl. Catal. A 147 (1996) 1259.
[12] R.D. Hetterley, R. Mackey, J.T.A. Jones, Y.Z. Khimyak, A.M. Fogg, I.V. Kozhevnikov, J. Catal. 258 (2008) 250.
[13] M.J. Climent, A. Corma, S. Iborra, A. Velty, J. Mol. Catal. A Chem. 182–183 (2002) 327.
[14] J.I. DiCosimo, C.R. Apesteguia, M.J.L. Gines, E. Iglesia, J. Catal. 190 (2000) 261.
[15] J.I. DiCosimo, V.K. Diez, M. Xu, E. Iglesia, C.R. Apesteguia, J. Catal. 178 (1998) 499.
[16] V.K. Diez, C.R. Apesteguia, J.I. DiCosimo, Stud. Surf. Sci. Catal. 139 (2001) 303.
[17] Y.Z. Chen, C.M. Hwang, C.W. Liaw, Appl. Catal. A 169 (1998) 207.
[18] Y.Z. Chen, B.J. Liaw, H.R. Tan, K.L. Shen, Appl. Catal. A 205 (2001) 61.
[19] A.C.C. Rodrigues, J.L.F. Monteiro, Stud. Surf. Sci. Catal. 154 (2004) 2395.
[20] G. Waters, O. Richter, B. Kraushaar-Czarnetzki, Ind. Eng. Chem. Res. 45 (2006) 5701.
[21] J.I. DiCosimo, G. Torres, C.R. Apesteguia, J. Catal. 208 (2002) 114.
[22] S.G. Powell, A.T. Nielsen, J. Am. Chem. Soc. (1948) 3627.
[23] R.M. West, E.L. Kunkes, D.A. Simonetti, J.A. Dumesic, Catal. Today 5 (2008).
[24] S.M. de Lima, I.O. da Cruz, G. Jacobs, B.H. Davis, L.V. Mattos, F.B. Noronha, J. Catal. 257 (2008) 356.
[25] F. Romero-Sarria, J.C. Vargas, A.C. Roger, A. Kiennemann, Catal. Today 133 (2008) 149.
[26] V. Solinos, E. Rombi, I. Ferino, M.G. Cutrufello, G. Colon, J.A. Navio, J. Mol. Catal. A Chem. 204-205 (2003) 629.
[27] J.C. Serrano-Ruiz, J. Luettich, A. Sepulveda-Escribano, F.R. Reinoso, J. Catal. 241 (2006) 45.
[28] B.E. Spiewak, J. Shen, J.A. Dumesic, J. Phys. Chem. 99 (1995) 17640.
[29] H.O. Zhu, J.R. Kim, S.K. Ihm, Appl. Catal. B 86 (2009) 87.
[30] K.A. Pokrovski, A.T. Bell, J. Catal. 241 (2006) 276.
[31] J. Wambach, A. Baiker, A. Wokaun, Phys. Chem. Chem. Phys. 1 (1999) 5071.
[32] D. Bianchi, T. Chafik, M. Khalfallah, S.J. Teichner, Appl. Catal. A 112 (1994) 219.
[33] S.M. DeLima, A.M. Silva, U.M. Graham, G. Jacobs, B.H. Davis, L.V. Mattos, F.B. Noronha, Appl. Catal. A 352 (2009) 95.
[34] Y.T. Kim, E.D. Park, H.C. Lee, D. Lee, K.H. Lee, Appl. Catal. B (2009).
[35] K. Otsuka, Y. Wang, M. Nakamura, Appl. Catal. A 183 (1999) 317.
[36] S. Lippert, W. Baumann, K. Thomke, J. Mol. Catal. 69 (1991) 199.
[37] G.S. Salvapati, K.V. Ramanamurty, M. Janardanarao, J. Mol. Catal. 54 (1989) 9.
[38] R. Alcala, M. Mavrikakis, J.A. Dumesic, J. Catal. 218 (2003) 178.
[39] R.D. Cortright, R.R. Davda, J.A. Dumesic, Nature 418 (2002) 964.
[40] F. Al-Wadaani, E.F. Kozhevnikova, I.V. Kozhevnikov, J. Catal. 257 (2008) 199.
[41] M.G. Musolino, P. Maio, A. Donato, R. Pietropaolo, J. Mol. Catal. A Chem. 208 (2004) 219.
[42] J. Wang, T. Li, Collect. Czech. Chem. Commun. 64 (1998) 107.
[43] V.K. Diez, C.R. Apesteguia, J.I. DiCosimo, J. Catal. 240 (2006) 235.
[44] S. Abello, S. Dhir, G. Colet, J. Perez-Ramirez, Appl. Catal. A 325 (2007) 121.
[45] L. Melo, F. Chevalier, P. Magnoux, M. Guisnet, in: Proceedings of the XIII Iberoamerican Symposium on Catalysis, Segovia, Spain, 1992.
[46] A.S. Ndou, N.J. Coville, Appl. Catal. A 275 (2004) 103.
[47] K. Kreuzer, R. Kramer, J. Catal. 167 (1997) 391.
[48] H. Tsuji, F. Yagi, H. Hattori, H. Kita, J. Catal. 148 (1994) 759.
[49] J. Weitkamp, M. Hunger, U. Rymsa, Micropor. Mesopor. Mater. 48 (2001) 255.
[50] M.A. Natal-Santiago, J.M. Hill, J.A. Dumesic, J. Mol. Catal. A Chem. 140 (1999) 199.
[51] M.A. Natal-Santiago, M.A. Sanchez-Castillo, R.D. Cortright, J.A. Dumesic, J. Catal. 193 (2000) 16.
[52] J. Lopez, J. Valente, J.-M.C. Sanchez, F. Figueras, J. Catal. 208 (2002) 30.
[53] J. McMurry, Organic Chemistry, fifth ed., Brooks/Cole Pub. Co., Pacific Grove, 2000.
[54] D. Gamarra, A. Martinez-Arias, J. Catal. 263 (2009) 189.
[55] J.I. Gutierrez-Ortiz, B. Rivas, R. Lopez-Fonseca, J.R. Gonzalez-Velasco, J. Therm. Anal. Calorim. 80 (2005) 225.
[56] L. Cider, N.H. Schöön, Appl. Catal. 68 (1991) 191.

[57] M.S. Li, J.Y. Shen, Mater. Chem. Phys. 68 (2001) 204.
[58] Y. Kamimura, S. Sato, R. Takahashi, T. Sodesawa, T. Akashi, Appl. Catal. A 252 (2003) 399.
[59] P. Panagiotopoulou, D.I. Kondarides, X.E. Verykios, Appl. Catal. A 344 (2008) 45.
[60] C.D. Leitenburg, A. Trovarelli, J. Kaspar, J. Catal. 166 (1997) 98.
[61] J. Kondo, H. Abe, Y. Skata, K. Maruya, K. Domen, T. Onishi, J. Chem. Soc. Faraday Trans. 1 (84) (1988) 511.